Short Papers

A Three-Dimensional Unconditionally Stable ADI–FDTD Method in the Cylindrical Coordinate System

Chenghao Yuan and Zhizhang Chen

***Abstract*—An unconditionally stable finite-difference time-domain (FDTD) method in the cylindrical coordinate system is presented in this paper. In it, the alternating-direction-implicit (ADI) method is applied, leading to a cylindrical ADI–FDTD scheme where the time step is no longer restricted by the stability condition, but by the modeling accuracy. In difference from the conventional ADI method, in which the alteration is applied in each coordinate direction, the ADI scheme here performs alternations in the mixed coordinates so that only two alternations in solution marching are required at each time step in the three-dimensional formulation. In difference from its counterpart in the Cartesian coordinate system, the cylindrical ADI–FDTD includes an additional special treatment along the vertical axis of the cylindrical coordinates to overcome singularity. Theoretical proof of the unconditional stability is shown and numerical results are presented to demonstrate the effectiveness of the cylindrical algorithm in solving electromagnetic-field problems.**

***Index Terms*—Alternating-direction-implicit (ADI) method, cylindrical coordinate system, finite-difference time-domain (FDTD) method, unconditional stability.**

I. Introduction

The finite-difference time-domain (FDTD) method [1] has been widely used in solving electromagnetic problems due to its capability of precise predictions of field behaviors. By finite differencing Maxwell's equations, the field solutions at a current time step are deduced from the field values at the previous time steps in a recursive fashion. This recursive scheme can provide field information in both time and frequency domains if the excitation is of large bandwidth. The detailed theory and extensive applications are described in [2].

Although the FDTD is an effective method in solving electromagnetic problems, there are inherent modeling constraints that limit its applications to electrically small structures. One of them is the Courant–Friedrich–Lecy (CFL) stability condition. It requires that a time step be smaller than a certain limit to ensure numerical stability. For a conventional cylindrical FDTD method [3], [4], the time step Δt has to satisfy the following CFL condition [3]:

$$\Delta t \le \Delta t_{\mathrm{CFL}} = \frac{1}{u_{\max}\cdot\sqrt{\left(\frac{1}{\Delta r}\right)^2+\left(\frac{2}{\Delta r\cdot\Delta\phi}\right)^2+\left(\frac{1}{\Delta z}\right)^2}} \tag{1}$$

where $u_{\max}$ is the maximum phase velocity in the media being modeled and Δr, $\Delta\phi$, and Δz are the smallest spatial discretization steps in the radial, angular, and vertical directions, respectively. Equation (1) indicates that the time-step limit is related to the spatial steps, as well as the medium constitutive parameters.

To remove the CFL constraint, unconditionally stable schemes can be developed. To this end, the alternating-direction-implicit (ADI) FDTD method has recently been developed in the Cartesian coordinate system [5]–[7]. In this paper, the extension of the method to the cylindrical coordinate system is presented with addition of a special singularity treatment for field components on the vertical axis. Such a cylindrical ADI–FDTD method is particularly effective for solving axis-symmetric structures such as cylindrical cavity resonators. The analytical proof of the unconditional stability is shown and numerical results are provided to validate the proposed cylindrical ADI–FDTD method. Note that the three-dimensional (3-D) cylindrical ADI–FDTD is developed in this paper for modeling general structures that may require the presence of various different modes as the result of discontinuities in the azimuthal or ϕ-direction. The same ADI principle can also be easily applied to the two-dimensional (2-D) cylindrical FDTD technique for structures with body-of-revolution (BOR) symmetry of [2, Ch. 12] leading to significant savings in computational expenditures.

The paper is organized in the following manner. In Section II, formulations of the proposed cylindrical ADI–FDTD method are presented. In Section III, proof of the unconditional stability is provided. In Section IV, the pertinent numerical results are showed. Finally, in Section V, conclusions and discussions are made.

II. ADI–FDTD Formulations in the Cylindrical Coordinate System

In an isotropic lossless region with permittivity ε and permeability μ, the six scalar equations that relate the components of electric field $\mathbf{E}$ and magnetic field $\mathbf{H}$ in the cylindrical coordinate can be readily obtained from the cylindrical Maxwell's equation. For instance,

$$\varepsilon\frac{\partial E_z}{\partial t} = \frac{\partial(rH_\phi)}{r\partial r} - \frac{\partial H_r}{r\partial\phi}. \tag{2}$$

When treated with the finite-difference scheme, the above equation presents a singularity on the $r=0$ because of the $1/r$ term. As a result, the cylindrical ADI finite-difference formulations have to be derived in two separate situations: one for the field components off the $r=0$ axis and the other for the field components along the $r=0$ axis.

A. ADI–FDTD Formulations for Field Components Off the $r=0$ Axis

In this case, no singularity is present. The ADI principle, as described in [6] and [7], can be directly applied to (2), resulting in (3) and (4), shown at the bottom of the following page. The equations for the other components can be obtained in a similar way.

In (3) and (4), both the right-hand side (RHS) and the left-hand side (LHS) contain unknown field components. To solve them in a more effective way, they are simplified by appropriate rearrangements and substitutions, as described in [6]. For instance, one can obtain

$$-\left(\frac{\left(i+\frac{1}{2}\right)\cdot\Delta t^2}{4\cdot i\cdot\varepsilon\cdot\mu\cdot\Delta r^2}\right)E_z^{n+(1/2)}\left(i+1,\,j,\,k+\frac{1}{2}\right)$$
$$+\left(1+\frac{\Delta t^2}{2\cdot\varepsilon\cdot\mu\cdot\Delta r^2}\right)E_z^{n+(1/2)}\left(i,\,j,\,k+\frac{1}{2}\right)$$
$$-\left(\frac{\left(i-\frac{1}{2}\right)\cdot\Delta t^2}{4\cdot i\cdot\varepsilon\cdot\mu\cdot\Delta r^2}\right)E_z^{n+(1/2)}\left(i-1,\,j,\,k+\frac{1}{2}\right)$$

Manuscript received June 5, 2001; revised January 10, 2002. This work was supported by the National Science and Engineering Research Council of Canada.

The authors are with the Department of Electrical and Computer Engineering, Dalhousie University, Halifax, NS, Canada B3J 2X4 (e-mail: z.chen@dal.ca).

Digital Object Identifier 10.1109/TMTT.2002.803450.

0018-9480/02$17.00 © 2002 IEEE

$$
\begin{aligned}
&= E_z^n\left(i,\, j,\, k+\frac{1}{2}\right) + \frac{\Delta t}{2\cdot\varepsilon\cdot i\cdot\Delta r} \\
&\cdot\left[\left(i+\frac{1}{2}\right)\cdot H_\phi^n\left(i+\frac{1}{2},\, j,\, k+\frac{1}{2}\right) - \left(i-\frac{1}{2}\right)\right. \\
&\quad \left.\cdot H_\phi^n\left(i-\frac{1}{2},\, j,\, k+\frac{1}{2}\right)\right] \\
&- \frac{\Delta t}{2\cdot i\cdot\varepsilon\cdot\Delta r\cdot\Delta\phi} \\
&\cdot\left[H_r^n\left(i,\, j+\frac{1}{2},\, k+\frac{1}{2}\right) - H_r^n\left(i,\, j-\frac{1}{2},\, k+\frac{1}{2}\right)\right] \\
&- \frac{\Delta t^2}{4\cdot i\cdot\varepsilon\cdot\mu\cdot\Delta z\cdot\Delta r} \\
&\cdot\left[\left(i+\frac{1}{2}\right)\cdot\left(E_r^n\left(i+\frac{1}{2},\, j,\, k+1\right) - E_r^n\left(i+\frac{1}{2},\, j,\, k\right)\right)\right. \\
&\quad - \left(i-\frac{1}{2}\right)\cdot\left(E_r^n\left(i-\frac{1}{2},\, j,\, k+1\right)\right. \\
&\qquad \left.\left. - E_r^n\left(i-\frac{1}{2},\, j,\, k\right)\right)\right]. \qquad (5)
\end{aligned}
$$

It forms a linear system of equations with a tri-diagonal coefficient matrix that can be solved in an efficient way.

B. ADI–FDTD Formulations for Field Components on the $r = 0$ Axis

In this case, as mentioned earlier, direct numerical updating of E_z from (2) is not feasible because of the $1/r$ term. To circumvent the difficulty, the following integral form of Maxwell's equation in the time domain is looked at and used:

$$\oint_c \overline{H}\cdot d\,\overline{l} = \varepsilon\cdot\int_s \frac{\partial\,\overline{E}}{\partial t}\cdot d\,\overline{s} \qquad (6)$$

where C is a closed contour surrounding the $r = 0$ axis, and S is the surface bounded by the contour C.

By using the closed circular path of radius $\Delta r/2$ around the $r = 0$ axis, the following non-ADI explicit finite-difference equation for E_z at $r = 0$ can be obtained [4]:

$$E_z^{n+1}(0,\, j,\, k) = E_z^n(0,\, j,\, k) + \frac{4\Delta t}{\varepsilon\cdot\Delta r}\, H_\phi^{n+(1/2)}\left(\frac{1}{2},\, j,\, k\right). \qquad (7)$$

To obtain the ADI formulations, the above equation is split into two sub time steps of computations as follows:

$$E_z^{n+(1/2)}(0,\, j,\, k) = E_z^n(0,\, j,\, k) + \frac{4\Delta t}{\varepsilon\cdot\Delta r}\, H_\phi^{n+(1/2)}\left(\frac{1}{2},\, j,\, k\right)$$

for the first sub time-step (8a)

and

$$E_z^{n+1}(0,\, j,\, k) = E_z^{n+(1/2)}(0,\, j,\, k) + \frac{4\Delta t}{\varepsilon\cdot\Delta r}\, H_\phi^{n+(1/2)}\left(\frac{1}{2},\, j,\, k\right)$$

for the second sub time-step. (8b)

$$
\begin{aligned}
&\frac{E_z^{n+(1/2)}\left(i,\, j,\, k+\frac{1}{2}\right) - E_z^n\left(i,\, j,\, k+\frac{1}{2}\right)}{\Delta t/2} \\
&= \frac{1}{\varepsilon\cdot i\cdot\Delta r}\left[\frac{\left(i+\frac{1}{2}\right)\cdot\Delta r\cdot H_\phi^{n+(1/2)}\left(i+\frac{1}{2},\, j,\, k+\frac{1}{2}\right) - \left(i-\frac{1}{2}\right)\cdot\Delta r\cdot H_\phi^{n+(1/2)}\left(i-\frac{1}{2},\, j,\, k+\frac{1}{2}\right)}{\Delta r}\right. \\
&\qquad \left. - \frac{H_r^n\left(i,\, j+\frac{1}{2},\, k+\frac{1}{2}\right) - H_r^n\left(i,\, j-\frac{1}{2},\, k+\frac{1}{2}\right)}{\Delta\phi}\right] \text{ at the first half time step (i.e., at the } (n+1/2)\text{th time step)}
\end{aligned}
\qquad (3)
$$

and

$$
\begin{aligned}
&\frac{E_z^{n+1}\left(i,\, j,\, k+\frac{1}{2}\right) - E_z^{n+(1/2)}\left(i,\, j,\, k+\frac{1}{2}\right)}{\Delta t/2} \\
&= \frac{1}{\varepsilon\cdot i\cdot\Delta r}\left[\frac{\left(i+\frac{1}{2}\right)\cdot\Delta r\cdot H_\phi^{n+(1/2)}\left(i+\frac{1}{2},\, j,\, k+\frac{1}{2}\right) - \left(i-\frac{1}{2}\right)\cdot\Delta r\cdot H_\phi^{n+(1/2)}\left(i-\frac{1}{2},\, j,\, k+\frac{1}{2}\right)}{\Delta r}\right. \\
&\qquad \left. - \frac{H_r^{n+1}\left(i,\, j+\frac{1}{2},\, k+\frac{1}{2}\right) - H_r^{n+1}\left(i,\, j-\frac{1}{2},\, k+\frac{1}{2}\right)}{\Delta\phi}\right] \text{ at the second half time step (i.e., at the } (n+1)\text{th time step)}
\end{aligned}
\qquad (4)
$$

TABLE I
SIMULATION RESULTS WITH DIFFERENT TIME STEPS

Analytical solution (GHz)	Δt	ADI-FDTD		FDTD	
		Resonant frequency (GHZ)	Relative error (%)	Resonant frequency (GHZ)	Relative error (%)
4.950	Δt_{CFL}	4.931	-0.38%	4.969	+0.38
	$4\Delta t_{CFL}$	4.960	+0.21	N/A	N/A
	$8\Delta t_{CFL}$	4.920	-0.60	N/A	N/A
	$12\Delta t_{CFL}$	4.916	-0.68	N/A	N/A

Again, they can be further simplified in the same way as described in [6]. Equation (8a) then becomes

$$-\frac{\Delta t^2}{\varepsilon\cdot\mu\cdot\Delta r^2}E_z^{n+(1/2)}(1,\,j,\,k)+\left(1+\frac{\Delta t^2}{\varepsilon\cdot\mu\cdot\Delta r^2}\right)\cdot E_z^{n+(1/2)}(0,\,j,\,k)$$
$$=E_z^n(0,\,j,\,k)+\frac{\Delta t}{\varepsilon\cdot\Delta r}H_\phi^n\left(\frac{1}{2},\,j,\,k\right)-\frac{\Delta t^2}{\varepsilon\cdot\mu\cdot\Delta r\cdot\Delta z}\left[E_r\left(\frac{1}{2},\,j,\,k+1\right)-E_r\left(\frac{1}{2},\,j,\,k\right)\right]. \quad (9)$$

Since (8b) is actually an explicit equation, there is no need to simplify it. Ez can be updated directly with the fields components at the previous time step.

III. ANALYTICAL PROOF OF THE UNCONDITIONAL STABILITY OF THE PROPOSED FDTD SCHEME

In the cylindrical coordinate system, six electric- and magnetic-field components in the spectral domain can always be expressed as [8]

$$E_r|_{i+(1/2),\,m,\,k}^n=E_r^nB_p\left(k_r\left(i+\frac{1}{2}\right)\Delta r\right)e^{jpm\Delta\phi}e^{jk_zk\Delta z}$$
$$H_r|_{i,\,m+(1/2),\,k+(1/2)}^n=H_r^nB_p(k_ri\Delta r)e^{jp(m+(1/2))\Delta\phi}e^{jk_z(k+(1/2))\Delta z}$$
$$E_\phi|_{i,\,m+(1/2),\,k}^n=E_\phi^nB_p(k_ri\Delta r)e^{jp(m+(1/2))\Delta\phi}e^{jk_zk\Delta z}$$
$$H_\phi|_{i+(1/2),\,m,\,k+(1/2)}^n=H_\phi^nB_p\left(k_r\left(i+\frac{1}{2}\right)\Delta r\right)e^{jpm\Delta\phi}e^{jk_z(k+(1/2))\Delta z}$$
$$E_z|_{i,\,m,\,k+(1/2)}^n=E_z^nB_p(k_ri\Delta r)e^{jpm\Delta\phi}e^{jk_z(k+(1/2))\Delta z}$$
$$H_z|_{i+(1/2),\,m+(1/2),\,k}=H_z^nB_p\left(k_r\left(i+\frac{1}{2}\right)\Delta r\right)e^{jp(m+(1/2))\Delta\phi}e^{jk_z\Delta z} \quad (10)$$

where $B_p(k_rr)$ is the appropriate Bessel function with k_r, $k\phi$, and k_z being the spatial frequencies along the r-, ϕ-, and z-direction, respectively.

By substituting the above expressions into the ADI equations, one can obtain two sets of matrix expressions for each of the two sub time steps, respectively,

$$X^{n+(1/2)}=\Lambda_1\cdot X^n \quad (11)$$
$$X^{n+1}=\Lambda_2\cdot X^{n+(1/2)} \quad (12)$$

or simply

$$X^{n+1}=\Lambda\cdot X^n \quad (13)$$

with $\Lambda=\Lambda_1\cdot\Lambda_2$.

By checking the magnitudes of the eigenvalues of Λ, one can determine whether the proposed scheme is unconditionally stable; if the magnitudes of all the eigenvalues of Λ are equal to or less than unity, the proposed scheme is unconditionally stable; otherwise it is potentially unstable [9].

Λ can be easily obtained by using a mathematical software, such as Maple V [10]. However, direct finding of its eigenvalues is very difficult. Therefore, an indirect approach is used with which the ranges of the eigenvalues can be determined. In this case, the Schur–Cohn–Fujiwa criterion (as described in [11]) is applied, where the characteristic polynomial of Λ, with its roots being the eigenvalues, is examined.

The Schur–Cohn–Fujiwa criterion states the following. If an nth-order polynomial is expressed in the following form:

$$F(z)=\sum_{i=0}^{n}a_iz^i,\qquad a_n>0 \quad (14)$$

and an $n\times n$ symmetric matrix $C=[\gamma_{ij}]$ being constructed with the elements

$$\gamma_{ij}=\sum_{p=1}^{\min(i,\,j)}\left(a_{n-i+p}a_{n-j+p}-a_{i-p}a_{j-p}\right) \quad (15)$$

then the number of the roots of $F(z)$ with their magnitudes being less than unity is equal to the number of positive eigenvalues of symmetric matrix C; the number of the roots of $F(z)$ with their magnitudes being larger than unity is equal to the number of negative eigenvalues of symmetric matrix C; the number of the roots of $F(z)$ with their magnitudes being exactly unity is equal to the number of **zero** eigenvalues of symmetric matrix C.

By using Maple V, the characteristic polynomial of Λ is found to be a sixth-order polynomial $(n=6)$

$$Z^6+B_5Z^5+B_4Z^4+B_3Z^3+B_4Z^2+B_5Z+1=0 \quad (16)$$

where $B_3 = A_3/A_6$, $B_4 = A_4/A_6$, $B_5 = A_5/A_6$, and B_α ($\alpha = 3, 4, 5$) are the coefficients of the characteristic polynomial. The expressions of A_α ($\alpha = 3, 4, 5, 6$) are very long and are not listed due to the limit of space.

Note that the coefficients of (16) are symmetric: the coefficient for the sixth-order term is the same as that for the zeroth-order term, the coefficient for the fifth-order term is the same as that for the first-order term, and the coefficient for the fourth-order term is the same as that for the second-order term. In other words, $a_6 = 1$, $a_5 = B_5$, $a_4 = B_4$, $a_3 = B_3$, $a_2 = B_4$, $a_1 = B_5$, and $a_0 = 1$. The corresponding C matrix is then a 6×6 zero matrix and all of the eigenvalues of C are **zeros**. Consequently, all the roots of (16), which are also the eigenvalues of Λ, reside on the unit circle on a complex plane with their magnitudes being unity. Therefore, the proposed cylindrical ADI–FDTD is unconditionally stable. The CFL stability condition no longer exists with the cylindrical ADI–FDTD method.

IV. Numerical Results

To numerically validate the ADI–FDTD scheme, two resonator structures are computed. They are: 1) a cylindrical cavity and 2) a cylindrical dielectric resonator. In both cases, simulations were run up to 100 000 iterations with a time step of four times of the CFL limit to see if the numerical solutions become divergent. No divergence was observed. As a result, the unconditional stability is numerically verified. Other aspects of the results are discussed below.

1) Circular Cylindrical Cavity: A simple cylindrical cavity resonator, whose analytical solutions are readily available [12], was computed. The radius of the cavity resonator is 3.995 cm and the height is 7.910 cm. The cavity is discretized with a uniform grid of $16 \times 16 \times 15$ along r, ϕ, and z, respectively. The electric field E_z is recorded at the grid point $(8, 8, 10)$ in both methods.

Table I presents the simulation results with 5000 iterations for the TE_{011} mode of the cavity with the increased time steps. Similar to its counterpart in the rectangular coordinate system [6], the cylindrical ADI–FDTD is found to have the increased errors with the increase of the time steps.

To assess the CPU time saving with the ADI–FDTD method, the cavity was also computed with the conventional cylindrical FDTD [3], [4] with $\Delta t = \Delta t_{\mathrm{CFL}}$ for the purpose of comparisons. By trial and error, it was found that the computational accuracies can be at the same level for both methods when $\Delta t = 4\Delta t_{\mathrm{CFL}}$ is used with the ADI–FDTD method. Consequently, to make the same of the actual physical time simulated with both methods, 20 000 iterations were selected with the FDTD and 5000 with the ADI–FDTD, respectively. The CPU time for the two methods was then found to be different: 267.27 s with the conventional FDTD and 66.32 s with the proposed method, on an AMD-Athlon950 computer. Roughly speaking, a saving factor of four was obtained with the proposed method in CPU time in this case.

In terms of the computation memory, the memory required by the cylindrical ADI–FDTD is almost double of that by the conventional FDTD, a result similar to the one presented in [6] and [7].

2) Cylindrical Dielectric Disk Resonator Enclosed With a Cylindrical Cavity: The second example computed is a cylindrical dielectric disk resonator enclosed with a cylindrical cavity (as shown Fig. 1). The whole region is discretized with a uniform $15 \times 16 \times 16$ mesh and the time step was taken to be four times the CFL limit. The resonant frequency computed with different methods was compared, and is shown in Table II. The resonant frequency obtained with the cylindrical ADI–FDTD scheme is found to agree well with those obtained with other methods. The differences among all the different methods are less than 1% this time.

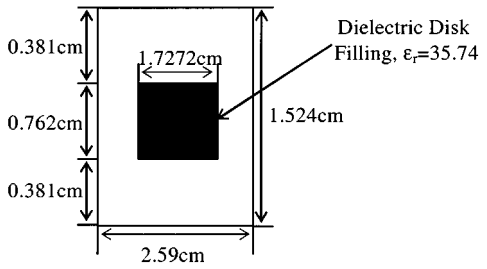

Fig. 1. Geometry of the dielectric disk resonator.

TABLE II
Resonant Frequency of the Dielectric Disk Obtained With Different Methods

Conventional FDTD Method	Finite Element Method (listed in [13])	Nonorthogonal FDTD Method ([13])	Proposed ADI-FDTD Method
3.516 GHz	3.51 GHz	3.53 GHz	3.539 GHz

V. Conclusions

A 3-D ADI–FDTD method in the cylindrical coordinate system free of the CFL stability condition has been presented in this paper. The Yee's grid is used and the alternative direction implicit technique is applied to formulate the algorithm. Analytical proof of the unconditional stability is shown and numerical simulation results are presented to validate the method and to demonstrate its effectiveness. In the examples computed, it is found that the cylindrical ADI scheme can achieve up to four times of saving in CPU time in comparison with the conventional FDTD method. However, the memory requirement is almost double of that for the conventional FDTD method.

Acknowledgment

The authors would like to thank Dr. C. Li and Dr. J. Zhang, as well as the other members of the Wireless Research Laboratory, Dalhousie University, Halifax, NS, Canada, for their help and assistance.

References

[1] K. S. Yee, "Numerical solution of initial boundary value problems involving Maxwell's equations in isotropic media," *IEEE Trans. Antennas Propagat.*, vol. AP-14, pp. 302–307, May 1966.

[2] A. Taflove, *Computational Electromagnetics: The Finite-Difference Time-Domain Method*. Norwood, MA: Artech House, 1996.

[3] N. Dib, T. Weller, and M. Scardelletti, "Analysis of 3-D cylindrical structures using the finite difference time-domain method," in *IEEE MTT-S Int. Microwave Symp. Dig.*, Baltimore, MD, May 1998, pp. 925–928.

[4] Y. Chen, Y. Chen, R. Mittra, and P. Harms, "Finite-difference time-domain algorithm for solving Maxwell's equations in rotationally symmetric geometries," *IEEE Trans. Microwave Theory Tech.*, vol. 44, pp. 832–839, June 1996.

[5] T. Namiki and K. Itoh, "A new FDTD algorithm free from the CFL condition restrain for a 2D-TE wave," in *IEEE AP-S Int. Symp. Dig.*, Orlando, FL, July 1999, pp. 192–195.

[6] F. Zheng, Z. Chen, and J. Zhang, "Toward the development of a three-dimensional unconditionally stable finite-difference time-domain method," *IEEE Trans. Microwave Theory Tech.*, vol. 48, pp. 1550–1558, Sept. 2000.

[7] T. Namiki, "3D ADI–FDTD method-unconditionally stable time-domain algorithm for solving full-vector Maxwell's equations," *IEEE Trans. Microwave Theory Tech.*, vol. 48, pp. 1743–1748, Oct. 2000.

[8] R. F. Harrington, *Time–Harmonic Electromagnetic Fields*. New York: McGraw-Hill, 1961.

[9] G. D. Smith, *Numerical Solution of Partial Differential Equations*. Oxford, U.K.: Oxford Univ. Press, 1978.
[10] M. B. Monagan and J. S. Devitt, *Maple V Programming Guide*. New York: Springer-Verlag, 1978.
[11] E. I. Jury, *Inners and Stability of Dynamic Systems*. New York: Wiley, 1974.
[12] D. M. Pozar, *Microwave Engineering*. Reading, MA: Addison-Wesley, 1990.
[13] P. H. Harms, J.-F. Lee, and R. Mittra, "A study of nonorthogonal FDTD method versus the conventional FDTD technique for computing resonant frequencies of cylindrical cavities," *IEEE Trans. Microwave Theory Tech.*, vol. 41, pp. 668–676, May 1993.

Hybrid Planar NRD-Guide Magic-Tee Junction

Yves Cassivi and Ke Wu

***Abstract*—A new magic-tee circuit is proposed and developed, which is based on the hybrid integration technology of a planar and nonradiative dielectric (NRD) guide. The magic-tee junction combines an NRD-guide T-junction with a microstrip T-junction. Furthermore, $\mathrm{LSM_{10}}$-mode radiators are introduced in the magic-tee circuit to reduce its resonance problem. Measured results show that an isolation of 20 dB can easily be achieved between the sum and difference ports.**

***Index Terms*—Hybrid planar/nonradiative dielectric (NRD) guide technology, magic-tee junction, millimeter-wave technology, mode suppressor, nonradiative dielectric (NRD) waveguide.**

I. Introduction

The nonradiative dielectric (NRD) waveguide is a promising technology for millimeter-wave applications. Various types of NRD-guide components have been proposed and developed [1], including filters, couplers, antennas, and hybrid planar NRD circuits [2]. In the latter case, the NRD-guide is coupled to a planar structure, e.g., a microstrip line, thereby combining and deploying the advantages of each individual design platform. However, there are no NRD-guide-based magic-tee junctions reported thus far in the literature. We propose a magic-tee junction that uses an NRD-guide T-junction combined with a microstrip T-junction.

In an NRD-guide, the two fundamental hybrid modes are the LSE_{10} and LSM_{10} modes. The LSM_{10} mode is usually preferred because it has a low-loss transmission property and it is the dominant TM_y-type mode, while the LSE_{10} mode is the second TE_y mode after the LSE_{00} mode. Mode conversion between the LSE_{10} and LSM_{10} modes is omnipresent in NRD-guide bends [3] and misalignments [4]. Yoneyama *et al.* [3] have developed a useful relationship between the radius of bend and the conversion loss for the LSM_{10} mode. This analysis shows that, for a very sharp bend, the LSM_{10} mode can almost completely be converted into its LSE_{10} counterpart. For this reason, the development of NRD-guide T-junctions [5]–[7] has led to a topology that was optimized for the complete modal conversion of an LSM_{10}-mode input signal into two equal LSE_{10}-mode signals at the output ports. It was also shown that a T-junction splitting an LSE_{10} mode into two LSM_{10} signals is also feasible [7]. A useful property of that type of NRD-guide T-junctions is the phase difference between the two outputs. Due to the electromagnetic field configuration of the LSE_{10} and LSM_{10} modes, an LSM_{10}-to-LSE_{10}-mode conversion T-junction will have 180° phase difference between the two outputs, but an LSE_{10}-to-LSM_{10}-mode conversion T-junction will have 0° phase difference between the two outputs. This is equivalent to the E- and H-plane rectangular waveguide T-junctions. Since the microstrip T-junction has an in-phase output signal, the NRD-guide LSM_{10}-to-LSE_{10}-mode conversion T-junction is adopted for the proposed magic-tee junction.

In this paper, a practical hybrid planar/NRD-guide magic tee is described first and then analyzed. It is shown that a resonance problem within the magic-tee junction appears when microstrip-to-NRD-guide transitions are placed at the three NRD-guide ports of the magic tee. Thus, an LSM_{10}-mode load is introduced to resolve this problem. The load does not affect the LSE_{10} mode and its construction is compatible with the hybrid planar/NRD-guide technology. Simulation and measurement results for the proposed magic tee are presented.

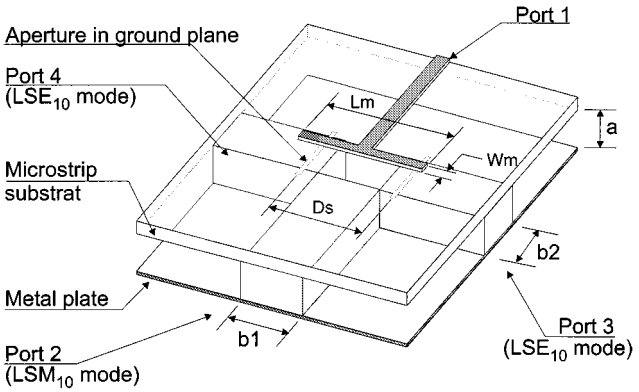

Fig. 1. Hybrid planar/NRD-guide magic-tee junction topology.

II. Hybrid Planar/NRD-Guide Magic-Tee Junction

The proposed magic-tee junction topology consists of an NRD-guide T- junction combined with a planar junction. The first option is to use a microstrip T-junction that has in-phase outputs with an NRD-guide LSM_{10}-to-LSE_{10} T-junction. The second approach is to use an NRD-guide LSE_{10}-to-LSM_{10} T-junction with a slotline-to-microstrip-line T-junction, the later having out of phase outputs. Only the first option is studied in this paper.

A. Proposed Topology for the NRD Magic-Tee Junction

Fig. 1 shows the proposed topology. The new magic tee is composed of an NRD-guide LSM_{10}-to-LSE_{10} T-junction, which is used as a difference port, and a microstrip junction used as a sum port. The microstrip T-junction and NRD-guide T-junction are combined with two microstrip-to-NRD-guide LSE_{10}-mode transitions [8]. The two transitions are placed over the two output branches of the NRD-guide T-junction. This arrangement produces two in-phase LSE_{10}-mode signals inside the output branches of the NRD-guide T-junction. Since two such signals are in phase, they cannot produce an LSM_{10}-mode signal at the difference port, contributing to a good isolation of the sum and difference ports. Similarly, the out-of-phase LSE_{10}-mode output signals produced by the NRD-guide T-junction generate a virtual short

Manuscript received July 31, 2001; revised January 8, 2002.
The authors are with the Poly-Grames Research Center, École Polytechnique de Montréal, Montréal, QC, Canada H3V 1A2 (e-mail: cassivy@grmes.polymtl.ca).
Digital Object Identifier 10.1109/TMTT.2002.803451.

0018-9480/02$17.00 © 2002 IEEE